AIAA SPACE 2009 Conference & Exposition
14 - 17 September 2009, Pasadena, California

AIAA 2009-6684

High Mass Mars Entry, Descent, and Landing Architecture Assessment

Bradley A. Steinfeldt,* John E. Theisinger,* Ashley M. Korzun,* Ian G. Clark,*
Michael J. Grant,* and Robert D. Braun†

Georgia Institute of Technology, Atlanta, GA 30332-0150

As the nation sets its sight on returning humans to the Moon and going onward to Mars, landing high mass payloads ($\geq$ 2 t) on the Mars surface becomes a critical technological need. Viking heritage technologies (*e.g.*, 70° sphere-cone aeroshell, SLA-561V thermal protection system, and supersonic disk-gap-band parachutes) that have been the mainstay of the United States' robotic Mars exploration program do not provide sufficient capability to land such large payload masses. In this investigation, a parametric study of the Mars entry, descent, and landing design space has been conducted. Entry velocity, entry vehicle configuration, entry vehicle mass, and the approach to supersonic deceleration were varied. Particular focus is given to the entry vehicle shape and the supersonic deceleration technology trades. Slender bodied vehicles with a lift-to-drag ratio (L/D) of 0.68 are examined alongside blunt bodies with L/D = 0.30. Results demonstrated that while the increased L/D of a slender entry configuration allows for more favorable terminal descent staging conditions, the greater structural efficiencies of blunt body systems along with the reduced acreage required for the thermal protection system affords an inherently lighter vehicle. The supersonic deceleration technology trade focuses on inflatable aerodynamic decelerators (IAD) and supersonic retropropulsion, as supersonic parachute systems are shown to be excessively large for further consideration. While entry masses (the total mass at the top of the Mars atmosphere) between 20 and 100 t are considered, a maximum payload capability of 37.3 t results. Of particular note, as entry mass increases, the gain in payload mass diminishes. It is shown that blunt body vehicles provide sufficient vertical L/D to decelerate all entry masses considered through the Mars atmosphere with adequate staging conditions for the propulsive terminal descent. A payload mass fraction penalty of approximately 0.3 exists for the use of slender bodied vehicles. Another observation of this investigation is that the increased aerothermal and aerodynamic loads induced from a direct entry trajectory (velocity ~6.75 km/s) reduce the payload mass fraction by approximately 15% compared to entry from orbital velocity (~4 km/s). It should be noted that while both IADs and supersonic retropropulsion were evaluated for each of the entry masses, configurations, and velocities, the IAD proved to be more mass-efficient in all instances. The sensitivity of these results to modeling assumptions was also examined. The payload mass of slender body vehicles was observed to be approximately four times more sensitive to modeling assumptions and uncertainty than blunt bodies.

Nomenclature

Variables

A	Effective projected vehicle area
C_D	Drag coefficient
C_L	Lift coefficient
$C_{m,\alpha}$	Pitching moment coefficient curve slope variation with angle-of-attack
C_T	Thrust coefficient
g_0	Earth's gravity constant ($g_0 = 9.806$ m/s^2)

*Graduate Research Assistant, Guggenheim School of Aerospace Engineering, AIAA Student Member
†David and Andrew Lewis Associate Professor of Space Technology, Guggenheim School of Aerospace Engineering, robert.braun@ae.gatech.edu, AIAA Fellow

I_{sp}	Specific impulse
L/D	Lift-to-drag ratio
m_0	Entry mass
$m_{backshell}$	Backshell mass
m_{cr}	Compression ring mass
m_{engine}	Engine mass
$m_{engine,RCS}$	Reaction control system engine mass
m_{gas}	Fill gas mass
$m_{heatshield}$	TPS portion of the heatshield mass
$m_{inflation}$	Inflation system mass
m_{IAD}	Tension cone inflatable aerodynamic decelerator mass
$m_{payload}$	Payload mass
$m_{prop,RCS}$	Reaction control system propellant mass
$m_{structure}$	Heatshield structure mass
m_{ts}	Tension shell mass
m_{tank}	Tank mass
p	Tank pressure
$\dot{q}$	Heat flux
$\bar{q}_{max}$	Maximum dynamic pressure
$\bar{q}_\infty$	Dynamic pressure ($\bar{q}_\infty = \frac{1}{2}\rho_\infty V_\infty^2$)
Q	Integrated heatload
r_n	Nose radius
s_{total}	Total vehicle surface area
s_{wet}	Wetted vehicle surface area
T	Fill gas temperature
$\bar{T}$	Engine thrust
V	Tank volume
V_∞	Free-stream velocity
α_T	Trim angle-of-attack
ϕ	Tank-mass factor
ρ_∞	Free-stream density

Acronyms and Abbreviations

CBAERO	Configuration Based Aerodynamics
CG	Center of Gravity
CH_4	Methane
DGB	Disk-Gap-Band
EDL	Entry, Descent, and Landing
EELV	Evolved Expendable Launch Vehicle
GA	Genetic Algorithm
HSIR	Human-Systems Interaction Requirement
IAD	Inflatable Aerodynamic Decelerator
LOx	Liquid Oxygen
MER	Mars Exploration Rovers
MSL	Mars Science Laboratory
OML	Outer Mold Line
PICA	Phenolic Impregnated Carbon Ablator
POST	Program to Optimize Simulated Trajectories
RCS	Reaction Control System
TPS	Thermal Protection System

I. Introduction

In 2008, NASA successfully landed its sixth robotic mission on the Martian surface. Each of these past missions have been characterized by the following:[1]

- A landed mass less than 600 kg
- A landed elevation less than -1.4 km MOLA
- A Viking heritage, 70° sphere-cone aeroshell
- A low lift-to-drag (L/D) ratio (four were ballistic, $L/D = 0$, and the remaining two had an $L/D = 0.18$)
- A Viking heritage, Disk-Gap-Band (DGB) parachute with diameter less than 16 m
- A Viking heritage, SLA-561V thermal protection system (TPS)
- No hypersonic entry guidance

Relative to these successes, the Mars Science Laboratory (MSL) mission, planned to launch in 2011, will take a large step forward in Mars entry, descent, and landing (EDL) technology. MSL will land a $\sim$ 950 kg payload at a surface elevation as high as 0 km MOLA using an entry system consisting of Phenolic Impregnated Carbon Ablator (PICA) TPS, hypersonic bank-to-steer guidance, a 4.5 m diameter, 70° sphere-cone aeroshell generating an L/D of $\sim$ 0.24, and a 21.5 m supersonic DGB parachute.

Future robotic missions are anticipated to have landed masses on the order of 1-2 t[1] and it is estimated that a human Mars mission will require surface elements that are on the order of 80 t.[2,3] In order to achieve these goals, a more capable EDL system must be developed. As outlined by Braun and Manning,[1] without some combination of the following—decreasing the hypersonic ballistic coefficient, extending the established supersonic parachute deployment region, moving to a more effective supersonic decelerator, or increasing the vertical lift of the entry vehicle, landing a mass as low as 2 t on the Martian surface may be infeasible.

The purpose of this investigation is to analyze appropriate EDL technologies that could be implemented in order to land high mass payloads on the surface of Mars. Two principal system trades are considered—entry vehicle shape and supersonic deceleration technology. The entry vehicle's shape and configuration affect the vehicle L/D, and, in general, with increasing vertical L/D the altitude at which a given Mach number is achieved increases (*e.g.*, the altitude at which the system can stage to supersonic deceleration can be raised). The Viking heritage DGB parachute was qualified to deploy between Mach 1.4 and 2.1, at dynamic pressures between 250 and 700 Pa, and with diameters up to 19.7 m.[4] Larger parachutes, such as those required by landing higher mass payloads on Mars, are likely to require fundamental requalification as the physical parameters which govern their performance (Mach number, dynamic pressure, diameter, material strength and temperature capabilities) are likely to be outside of the Viking technology box.[1] Furthermore, the aerothermal limits of parachute materials will likely impose an upper limit on the deployment Mach number in the Mach 2.5 - 3.0 range. Therefore, in this investigation, two supersonic deceleration technologies which have shown potential for higher payload masses are studied—inflatable aerodynamic decelerators (IAD)[5] and supersonic retropropulsion.[6]

II. Mars Entry, Descent, and Landing Design Space

There are several inherent architectural trades associated with landing high mass vehicles on the surface of Mars. These trades are shown in Table 1 where italicized items are assumed for this investigation, items in gray are not considered, and all other items are traded. The assumed parameters include a 10 m constraint on the entry vehicle diameter imposed by the maximum payload shroud diameter of any foreseen launch vehicle, the Ares V. For orbital entry velocities, it is assumed that the entry system is placed into Martian orbit using propulsion to avoid any existing aerothermal load on the vehicle. This assumption is consistent with current NASA studies.[3] Instead of implementing closed-loop guidance which is sensitive to vehicle modeling assumptions, an optimal bank profile is computed in which bank angle values are assigned at eight discrete Mach numbers in the hypersonic regime. These bank angles are design variables within the system optimization so that the maximum payload mass trajectory is obtained. In addition, this investigation effectively finds a lower bound for the propellant mass fraction by assuming a constant thrust gravity turn guidance law initiated at Mach 0.8 or 5 km, whichever is a lower altitude. The gravity turn does not target a specific landing site, but does ensure a soft landing on the surface is achieved by thrusting opposite to the vehicle's velocity vector. As such, the results presented in this investigation represent a feasible upper bound on system performance. For example, inclusion of a targeted pinpoint landing capability would result in a larger propellant mass fraction and a reduced payload mass fraction.[7] Similarly, inclusion of environmental, vehicle and navigation uncertainties would further constrain predicted performance.

The first item in Table 1 traded is the velocity at which the vehicle first enters the atmosphere. Two velocities are considered, 4 km/s and 6.75 km/s, with the lower velocity representing entry from orbit and

Table 1. High mass EDL design space.

Arrival Architecture	Split	All-in-one	
Launch Vehicle	*10 m Diameter Launch Shroud Constrained (Ares V)*	> 10 m Diameter (Large EELV)	
Mars Orbit Insertion	*Propulsive*	Aerocapture	
Entry Velocity	Orbital (4 km/s)	Medium (5.5 km/s)	Direct (6.75 km/s)
Entry Configuration	Blunt Rigid ($L/D \sim 0.3$)	Slender Rigid ($L/D \sim 0.7$)	
Entry Mass	3 t (MSL Like)	20 t - 100 t	
Packaging Density	Range of 10-400 kg/m^3		
Bank Profile	*Optimized*	Guided	
Supersonic Deceleration	Parachute	IAD	Supersonic Retropropulsion
Hazard Avoidance	Divert	*None*	
Terminal Descent	*Constant Thrust Gravity Turn*	Targeted Landing Site Guidance	
Touchdown	Propulsive Fixed Below Payload	Propulsive Fixed Above Payload	

the higher velocity representing entry directly from the interplanetary transfer from Earth. Ultimately, this is a trade on launch vehicle capability as additional mass would need to be included for the vehicle to enter orbit about Mars, whether it is in inserted via an aeroassist maneuver or a purely propulsive maneuver. The entry vehicle's shape and configuration is one of the fundamental trades that this investigation addresses. A blunt rigid body, such as a sphere-cone or capsule, has heritage at Mars and in human spaceflight, whereas a slender body, such as a biconic or ellipsled, does not. However, there may be a condition where the blunt body cannot provide sufficient vertical lift and thus cannot adequately land sufficient payload on the Martian surface. This investigation attempts to address this question by modeling a representative blunt body and slender body—the 70° sphere-cone and the ellipsled, respectively.

The next two items traded in the design space are correlated, entry mass and packaging density. Payload elements for future Mars missions have been surmised to be as massive as 20 to 80 t.[1,3] Entry masses for such large payload masses are likely to be two to three times this value. Packaging density provides a volumetric constraint on mass as packaging densities are thought to be constrained to that of Apollo Command Module, at 350 kg/m^3 for a larger class vehicle.[8] Table 2 shows the packaging density for each entry mass investigated for the two different aeroshell shapes considered. In this analysis, the aeroshells are sized to the maximum available launch vehicle shroud diameter of 10 m. Smaller aeroshells lead to higher packaging densities than that shown in Table 2. Note that the highest packaging densities correspond to the sphere-cone aeroshell, and based on the Apollo packaging density constraint any entry mass greater than approximately 86 t for the sphere-cone may be unachievable.

The other fundamental design space trade addressed in this investigation is the method of supersonic deceleration. Here, an attached tension cone IAD is traded against variable-thrust supersonic retropropulsion executed with a gravity turn control law.

Table 2. Packaging densities for various entry masses.

Entry Mass	**10 m Diameter 70° Sphere-Cone Aeroshell**	**10 × 30 m Ellipsled**
20 t	80.9 kg/m^3	9.0 kg/m^3
40 t	161.8 kg/m^3	18.0 kg/m^3
60 t	242.7 kg/m^3	26.0 kg/m^3
80 t	323.6 kg/m^3	36.0 kg/m^3
100 t	*404.5 kg/m^3*	44.9 kg/m^3

III. Modeling

III.A. Aerodynamics and Stability

For this investigation, a hypersonic aerodynamics analysis of rigid entry aeroshells was performed using a Newtonian impact model. The body surface is divided into panels and the surface pressure coefficient is determined for each panel based on the surface normal vector. With the pressure distribution determined

over the entire body, the forces and moments are resolved through integration over the aeroshell surface area. Results generated were corroborated with a first-order industry standard tool, the configuration based aerodynamics (CBAERO) tool.[9]

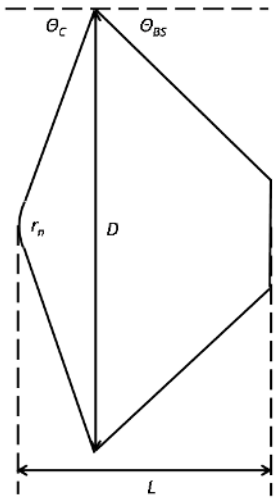

(a)

Parameter	Value
L	5.7 m
D	10 m
r_n	2.5 m
θ_C	70°
θ_{BS}	43.37°

Parameter	Value
α_T	-19.3°
L/D	0.3
C_L	0.427
C_D	1.424

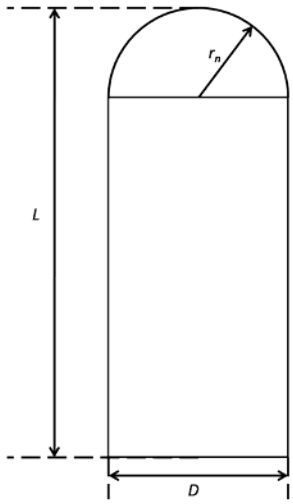

(b)

Parameter	Value
L	30 m
D	10 m
r_n	5 m

Parameter	Value
α_T	35°
L/D	0.68
C_L	1.179
C_D	1.713

Figure 1. Shape parameters for the (a) 10 m diameter 70° sphere-cone and (b) 10 × 30 m ellipsled.

For this analysis, two representative bodies are considered—a blunt body, the 70° sphere-cone with a similar outer model line (OML) to Mars Pathfinder,[10] and a slender body, a 10 × 30 m ellipsled with OML similar to that of the Mars Design Reference Architecture 5.0 investigation.[3] In order to represent the aerodynamic performance capability of these shapes, it is desired that the 70° sphere-cone produce an L/D of 0.30 (at a trim angle-of-attack, α_T, of -19.3°) and the ellipsled produce an L/D of 0.68 (α_T of 35.0°).

The range of possible center of gravity (CG) locations required to trim these aeroshells at their respective α_T is depicted by the trim lines shown in Figure 2. These trim lines are also shaded by color correlating to the value of $C_{m,\alpha}$ at each CG location. Note that for static stability, $C_{m,\alpha} < 0$. As such, the red region of each trim line indicates CG locations with less static stability. Unlike the sphere-cone, there are CG positions for the ellipsled which result in the vehicle being statically unstable. The stable CG positions for the ellipsled are generally farther from the centroid than for the sphere-cone, requiring greater non-uniformity in packaging its payload mass. From a packaging standpoint, the α_T required by the ellipsled may not be satisfied by the CG offset alone, and a trim tab or body flap may need to be implemented. However, the physical size of the ellipsled may be useful in accomodating large-volume payloads.

III.B. Trajectory

The hypersonic and supersonic portions of the trajectory were simulated using the Program to Optimize Simulated Trajectories (POST),[11] which is a generalized three degree-of-freedom trajectory, parameter targeting and optimization program. The POST terminal condition used is Mach 0.8, at which point a propulsive terminal descent begins if the altitude is less than 5 km, otherwise the vehicle's state is propagated to the staging altitude of 5 km and a propulsive terminal descent is begun. The propulsive terminal descent trajectory is simulated using a constant thrust gravity turn guidance law that targets a soft touchdown state ($h = 0$ km AGL, $V = 0$ m/s). The gravity turn control law commands thrust opposing the vehicle's atmosphere relative velocity vector. A constant thrust magnitude is iterated upon using a Newton iteration scheme. A thrust-to-weight limit of three is assumed (relative to Martian gravity) for the propulsive phase of flight. The nominal density and pressure profiles as reconstructed by the Mars Pathfinder mission are assumed.[10]

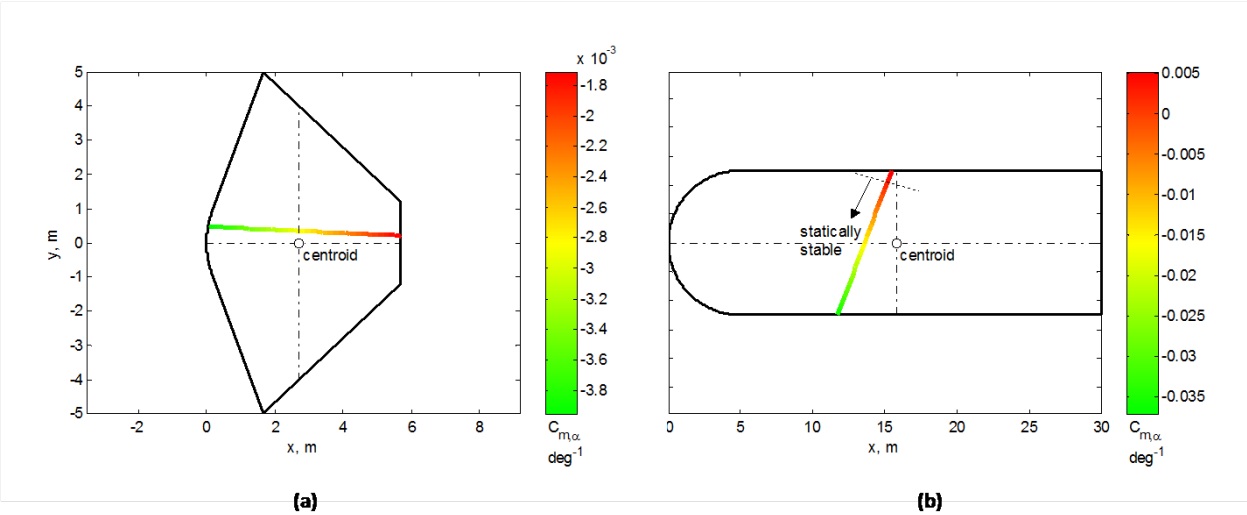

Figure 2. CG trim lines for the (a) 10 m diameter 70° sphere-cone and (b) 10 × 30 m ellipsled.

III.C. Subsystem Modeling and Sizing

III.C.1. Aerothermal Environment

Heating Models

For Mars missions prior to MSL, peak heating occurred under laminar conditions at the stagnation point. In such cases, a Sutton-Graves[12] type engineering correlation has been shown to reliably predict the heat flux experienced during the entry. However, turbulent conditions dominate at peak heating for MSL and the larger vehicles in this investigation, due to the large ballistic coefficient and running length of these systems. As a result, the heat flux and shear is substantially increased and the location of the peak heating shifts to the leeward shoulder of the vehicle.[13] Since all of the blunt vehicles considered in this investigation have a larger ballistic coefficient and diameter than MSL, a turbulent heating relationship is assumed. This relationship is developed using CBAERO, which in addition to its aerodynamics estimation capabilities, has the capability of providing conceptual aerothermodynamics estimates using engineering relationships.[9] At the stagnation point of the vehicle, a relationship based on Tauber[14] is utilized. Elsewhere on the vehicle, acreage heating is estimated based on Eckert's method.[9] Since the flowfield about a large ellipsled vehicle at Mars is largely unknown, this investigation assumes that the flowfield is turbulent at the peak heating location (due to the large running length of the vehicle). Using this assumption, a similar approach to that of the 70° sphere-cone is employed, again using CBAERO.

The models developed use the peak heat rate observed on the body for the given flow conditions. For example, at the conditions seen in Figure 3, a heat rate of 129.05 W/cm^2 would be used for the 10 m diameter, 70° sphere-cone and 120.93 W/cm^2 for the 10 × 30 m ellipsled. For a given trajectory, integrated heat load is obtained by integrating the observed heat flux through the entire trajectory.

Thermal Protection System Sizing

The TPS protects the vehicle from the harsh aerothermal environment during atmospheric entry. The principal TPS material used in previous Mars exploration missions has been SLA-561, having been used on Viking, Pathfinder, and the Mars Exploration Rovers (MER). PICA is planned for use on MSL.[15]

A first-order relationship determined by Laub and Venkatapathy[16] uses heat load as the sole parameter to determine the heatshield TPS mass fraction. This approximate relation is used in this investigation to size the TPS material for the heatshield. The model uses historical United States planetary missions at Venus, Earth, Mars, and Jupiter with ablative TPS to regress TPS mass fraction against the integrated heat load. These missions have integrated heat loads ranging from approximately 3 × 10^3 J/cm^2 to 2 × 10^5 J/cm^2 (the trajectories analyzed in this investigation have heat loads that are approximately 7-12 × 10^3 J/cm^2).

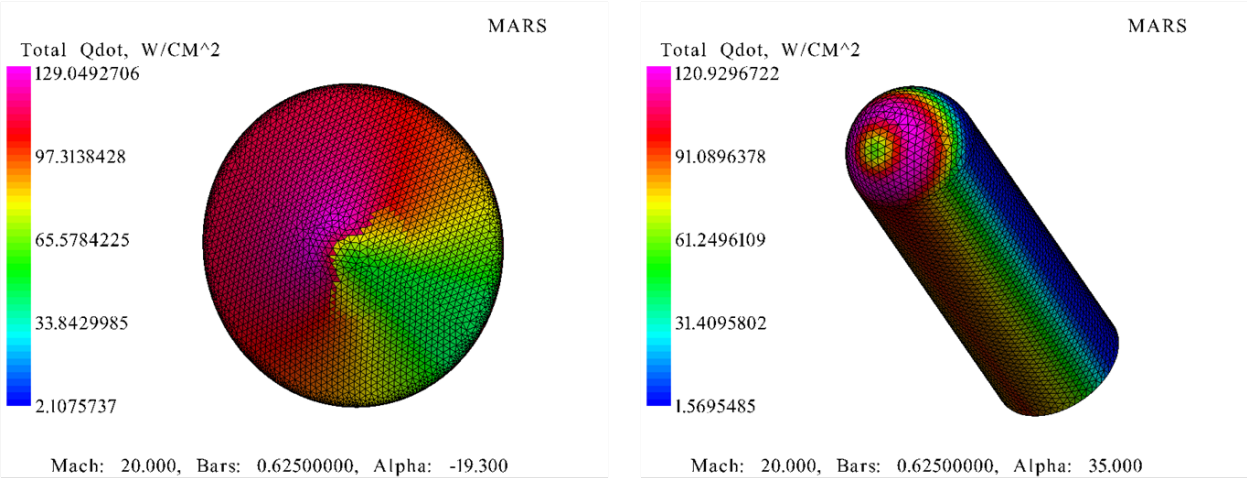

Figure 3. Sample heat flux distribution for the (a) 10 m diameter 70° sphere-cone and (b) 10 × 30 m ellipsled.

The derived mass model for the TPS portion of the forebody heatshield is given by[16]

$$m_{heatshield} = \left(0.00091 Q^{0.51575}\right) m_0 \tag{1}$$

where Q is the integrated heat load in J/cm^2 and m_0 is the entry mass. Two important observations should be noted about this relationship: (1) all of the missions used to regress this relationship are blunt body geometries, and (2) the TPS mass is assumed independent of TPS material.

III.C.2. Structure

Forebody Structure

In previous EDL system studies, the mass required for the forebody structure has been estimated using a single mass fraction without regard for the physics of the problem.[2,3,17,18] However, it is physically intuitive that this structural mass is dependent on the load placed on the vehicle. This relationship can be seen, in Figure 4, where the underlying structural mass fraction is regressed against peak dynamic pressure. The choice of peak dynamic pressure is a surrogate for the load placed on the heatshield (which the heatshield must accommodate without failure due to buckling or stress). It should be noted that the regression shown in Figure 4 is based on historical data from blunt entry bodies. Therefore, it provides an adequate mass estimating relationship for the sphere-cone. The mass of the heatshield substructure is given by

$$m_{structure}|_{blunt} = (0.0232 \bar{q}_{max}^{0.1708}) m_0 \tag{2}$$

where $\bar{q}_{max}$ is the peak dynamic pressure experienced during the entry in Pascals. Because of the increased area of the slender body, a multiplicative scaling factor is added to Eq. (2) to obtain the mass of the heatshield substructure for the ellipsled. This augmented equation is shown in Eq. (3)

$$m_{structure}|_{slender} = \left(\frac{s_{wet}|_{slender}}{s_{wet}|_{blunt}}\right)^{1/2} (0.0232 \bar{q}_{max}^{0.1708}) m_0 \tag{3}$$

where $s_{wet}|_{slender}$ is the wetted area at α_T for the slender body and is 349.1 m^2 in this investigation, and $s_{wet}|_{blunt}$ is the wetted area at α_T for the blunt body and is taken to be 83.5 m^2. Note that the scale exponent factor of $\frac{1}{2}$ is the same factor associated with the critical Euler buckling load for a pinned-pinned column.

Backshell

The backshell serves two primary purposes: as a structural member of the aeroshell, and as a means to

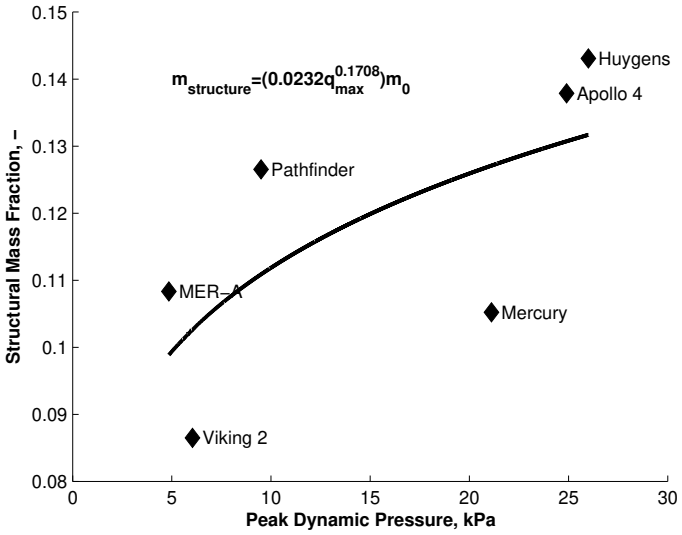

Figure 4. Dynamic pressure influence on underlying forebody structural mass fraction.

provide thermal protection for the flowfield around the aftbody. Past Mars robotic mission experience (Mars Pathfinder and MER) is leveraged to give a backshell mass estimating relationship for the sphere-cone of

$$m_{backshell}|_{blunt} = (0.14)m_0 \tag{4}$$

where 0.14 is the average of the backshell mass fractions (comprised of both TPS and structural mass) for the two missions. Once again, due to the increased surface area of the slender body, a scale factor is added to Eq. (4) to account for the increased *effective* backshell area of a slender vehicle

$$m_{backshell}|_{slender} = \left(\frac{(s_{total} - s_{wet})|_{slender}}{s_{backshell}|_{blunt}} \right)^{1/2} (0.14)m_0 \tag{5}$$

where the quantity $(s_{total} - s_{wet})|_{slender}$ is the non-wetted, *effective* backshell area of the slender body (593.4 m^2 in this case), and $s_{backshell}|_{blunt}$ is the backshell area of the sphere-cone, which is 105.8 m^2 in this investigation.

III.C.3. Supersonic Deceleration

Inflatable Aerodynamic Decelerators

By design, supersonic IADs are intended to increase the drag area of a vehicle at Mach numbers and dynamic pressures considerably higher than those possible using parachutes. This is a result of their increased drag effectiveness and improved structural efficiency. For this investigation, a tension cone IAD is assumed, as shown in Figure 5(a) for the 70° sphere-cone and in Figure 5(b) for the ellipsled.

In this investigation, the tension cone is deployed at Mach 5 by rapid inflation of the compression ring. The shell of the tension cone, with shape derived from a prescribed pressure distribution obtained using linear membrane theory,[4] is then unfurled with connections at the aeroshell and the compression ring. The compression ring must be able to withstand the compressive load seen from the pressure distribution over the shell, which determines its inflation pressure. Once a subsonic speed is reached, the tension cone is jettisoned and the vehicle transitions to its propulsive terminal descent configuration.

For this investigation, the tension shell is assumed to be made of Vectran, with the compression ring being inflated with nitrogen. The supersonic aerodynamics were established using inviscid CFD solutions and were shown to demonstrate good agreement with viscous CFD solutions and wind tunnel data.[19] The tension cone drag coefficient variation with Mach number is shown in Figure 6.

The mass of the tension cone is the summation of four separately sized elements: (1) the tension shell (m_{ts}), (2) the compression ring (m_{cr}), (3) the inflation gas (m_{gas}), and (4) the inflation system ($m_{inflation}$).

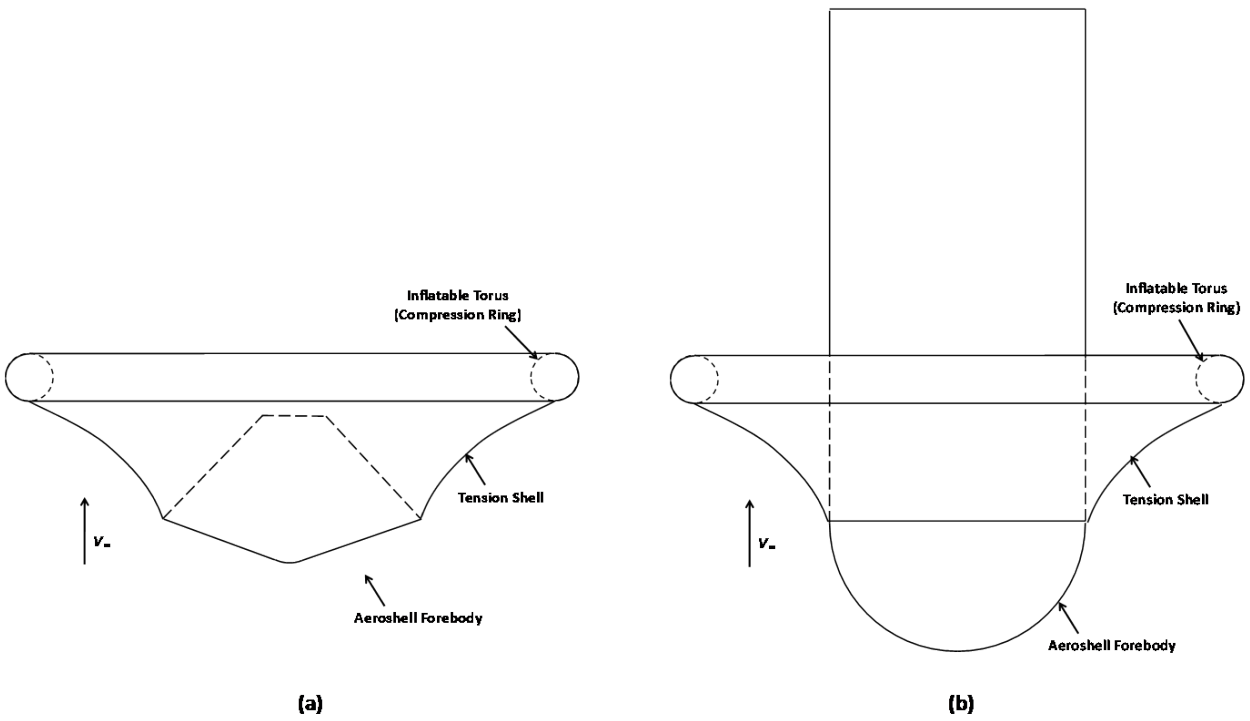

Figure 5. Geometry associated with a supersonic tension cone.

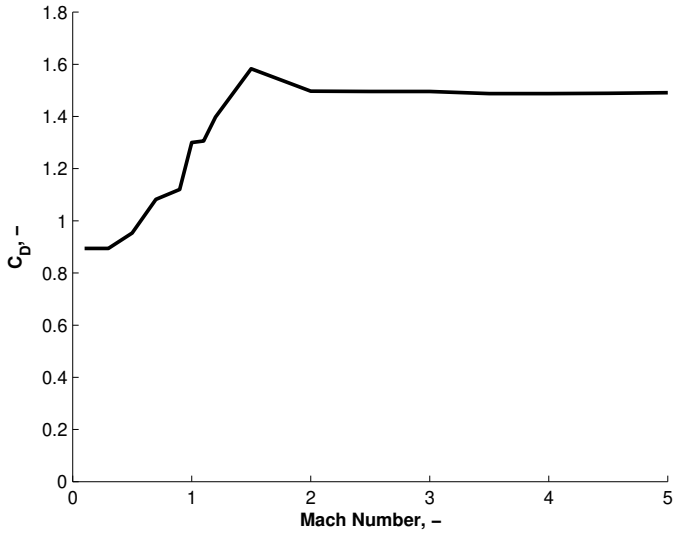

Figure 6. Tension cone drag coefficient variation with Mach.

Hence, the total mass of the tension cone IAD is given by

$$m_{IAD} = m_{ts} + m_{cr} + m_{gas} + m_{inflation} \tag{6}$$

Supersonic Retropropulsion

Retropropulsion as a means of supersonic deceleration has long been thought of as a concept for Mars EDL.[6] Interactions between the exhaust from retropropulsion nozzles and the blunt body shock structure surrounding the vehicle have been observed to significantly alter the static aerodynamic characteristics of

the vehicle.[20,21] Configurations with the nozzles at the periphery of the vehicle forebody have been shown to preserve and even retain most of the aerodynamic drag force. This is in contrast to the force trends observed for retropropulsion configurations with either a single nozzle or a cluster of multiple nozzles at the vehicle nose, where the aerodynamic drag coefficient was reduced to approximately 10% of its "no propulsion" value for any appreciable thrust level. The experimental database for supersonic retropropulsion is extremely limited in terms of available data on peripheral retropropulsion configurations, slender body geometries, scaling uncertainties, and potential aerothermal effects arising from high enthalpy retropropulsion exhaust.[6]

In this investigation, the vehicle configuration has been assumed to have multiple retropropulsion nozzles at the periphery of the vehicle forebody for consistency with existing experimental data.[20,21] A performance model accounting for aerodynamic-propulsive interactions was developed for cases initiating retropropulsion at supersonic conditions as a function of the thrust coefficient, C_T. The thrust coefficient is defined to be

$$C_T = \frac{\bar{T}}{\bar{q}_\infty A} \tag{7}$$

where $\bar{T}$ is the thrust of the engines, $\bar{q}_\infty$ is the free-stream dynamic pressure, and A is the effective projected area of the vehicle.

Consistent with experimentally observed force coefficient trends for a peripheral retropropulsion configuration, the aerodynamic drag coefficient model used for supersonic retropropulsion is shown in Figure 7.[22] Within the supersonic trajectory segment of flight, a profile of ten thrust coefficients is specified at ten

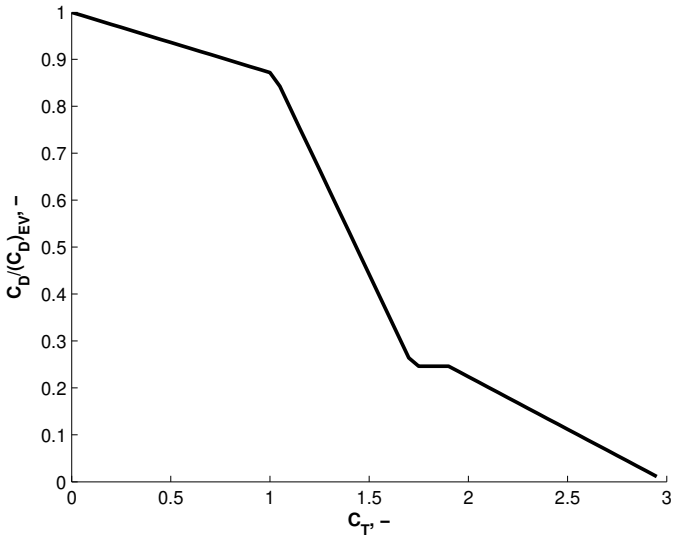

Figure 7. Drag coefficient variation with thrust coefficient for supersonic retropropulsion.

relative velocities. Based on the corresponding thrust coefficient, the force coefficients are altered to account for the propulsive-aerodynamic interaction. The additional propellant usage from this deceleration is simply added to the subsonic terminal descent propulsion system requirement.

III.C.4. Propulsion

The propulsion system used for the supersonic retropropulsion and terminal descent phase of flight is assumed to be a liquid bipropellant engine using liquid oxygen (LOx) and methane (CH_4), consistent with previous Mars studies.[2,3,17,18] LOx is assumed to have a density of 1142 kg/m^3 and CH_4 is assumed to have a density of 422.6 kg/m^3. The LOx/CH_4 engine is assumed to have a specific impulse of 350 seconds with a mixture ratio of 3.5. Based on past conceptual design work, a mass estimating relationship for the engine is derived as[2]

$$m_{engine} = (0.00144)\bar{T} + 49.6 \tag{8}$$

where the engine mass, m_{engine}, is given in kilograms and the thrust, $\bar{T}$, is in Newtons. Since a common system is utilized for both the supersonic retropropulsion and terminal descent, a common thrust-to-weight

constraint is imposed. This is the ratio of the engine thrust to the entry weight of the system and it is constrained to be less than three (relative to Martian gravity).

It is assumed that the propellant tanks are made of titanium and have an operating pressure near 1.4 MPa (corresponding to a burst pressure ∼2.8 MPa). The tank mass (in kilograms) for each of the tanks can be found as[23]

$$m_{tank} = \frac{pV}{g_0 \phi} \tag{9}$$

where p is the operating pressure of the propellant in Pascals, V is the volume of the LOx or CH_4 in cubic meters, g_0 is Earth's gravitational constant, and ϕ is the tank-mass factor, assumed to be 5000 m for titanium. Additionally, a 50% mass margin is applied to the tank mass in order to account for design uncertainty.

III.C.5. Reaction Control System

A notional reaction control system (RCS) is sized to perform the bank angle modulation during the hypersonic entry. The engine and storage tank mass is taken to be 0.5% of the entry mass,

$$m_{engine,RCS} = (0.005) m_0 \tag{10}$$

It is assumed that the RCS system is sized to provide 30 m/s of velocity change with a 200 second specific impulse. Therefore, the propellant for the RCS is given by the expression

$$m_{prop,RCS} = \left[1 - \frac{1}{exp\left(\frac{\Delta V}{g_0 I_{sp}}\right)} \right] m_0 = (0.0101) m_0 \tag{11}$$

where ΔV is the velocity change required, g_0 is Earth's gravity constant, and I_{sp} is the specific impulse of the engine.

III.C.6. System Margin

Given the conceptual nature of this investigation, two margins are applied to account for the uncertainty of the various concepts. The first is a dry mass margin, which is applied to the the mass of the vehicle's systems, neglecting the supersonic retropropulsion, terminal descent, and RCS propellant. This margin is taken to be 15%. Additionally, a 10% margin is applied to the propellant required to perform the vehicle's supersonic retropropulsion (if used) and terminal descent.

III.D. System Sizing Methodology

III.D.1. Size as You Fly Methodology

Traditionally, vehicle sizing is performed using an iterative process. The vehicle's initial state and mass of all of subsystems are specified at the beginning of the iteration. The trajectory is then simulated and the subsystem's mass estimates are updated based upon the vehicle's atmospheric flight profile. This process is repeated until the trajectory and subsystem masses converge. Using this methodology the mass of numerous subsystems must converge with the trajectory. In order to eliminate this iteration, a *size as you fly* methodology is implemented to perform the subsystem sizing for this investigation.

The size as you fly methodology requires only the total vehicle mass and geometry be specified at the beginning of the simulation. This total vehicle mass accounts for all of the subsystems; individual subsystems are sized only as the relevant events occur. By specifying a total vehicle mass and geometry, proper aerodynamic and gravitational forces are imparted on the vehicle at all stages throughout the trajectory without the need for iteration. As an example, consider the sizing of the heatshield. Immediately prior to jettisoning the heatshield, the heatshield is sized based on the heating data obtained through the trajectory simulation. This approach allows the heatshield to be sized for the specific trajectory flown and allows the appropriate mass loss to be applied accurately after jettison. At the termination of the simulation, each subsystem is sized to appropriately represent the physics experienced by the vehicle. The remaining unallocated mass corresponds to the total payload mass delivered to the surface.

III.D.2. Optimization Strategy

In this investigation, the payload mass on the surface of Mars is maximized subject to a set of flight mechanics and physical constraints. For this investigation, the constraints are taken to be the NASA Human-Systems Interaction Requirement (HSIR) deceleration limit for automated escape,[24] a peak heat rate less than 1200 W/cm^2, and a maximum skip altitude of 150 km should the vehicle exit the atmosphere during entry. The free parameters of the problem are then varied between their given ranges in order to arrive at an optimum solution. The design variables for vehicles containing an IAD include the entry flight path angle and eight hypersonic bank angle segments. For vehicles using supersonic retropropulsion, ten additional design variables are added—throttle settings at ten different relative velocities between 2000 and 200 m/s. To obtain the maximum payload mass design, a real-valued genetic algorithm is used.

III.E. System Sizing Comparisons

III.E.1. Mars Science Laboratory Class Mission

To validate the performance of the developed design tool to a fairly mature EDL system, the MSL mission's design as specified in early 2006[25] is used. The parameters for the two EDL systems in this comparison are shown in Table 3. Note that the flight path angle is removed from the optimization procedure. The results of this comparison are shown in Table 4. The present investigation's modified analysis tool replicates the MSL

Table 3. MSL class and replicated vehicle parameters.

	MSL Class Vehicle	**This Investigation**
Entry Vehicle Shape	70° Sphere-Cone	70° Sphere-Cone
Entry Vehicle Diameter	4.5 m	4.5 m
Hypersonic L/D	0.21	0.21
Entry Mass	2,616 kg	2,616 kg
Inertial Entry Velocity	6.3 km/s	6.3 km/s
Inertial Entry Flight Path Angle	-14°	-14°
Heating Regime	Laminar	Laminar
Heatshield TPS Material	SLA-561V	Heat Load Based Regression
Hypersonic Guidance	Apollo Final Phase (Bank-to-Steer)	Discrete Bank Angle Profile (Chosen by Optimizer)
Supersonic Deceleration	19.7 m DGB Parachute	19.7 m DGB Parachute
Propulsive Terminal Descent	Sky-Crane Terminal Descent Profile	Gravity Turn

Table 4. Comparison between MSL class and replicated vehicle sizing results.

	MSL Class Vehicle		**This Investigation**			
Component	*Mass [kg]*	$m_{component}/m_{entry}$	*Mass [kg]*	$m_{component}/m_{entry}$	*Mass Difference [kg]*	*% Difference*
Heatshield	516	0.197	476	0.182	-40	-7.84%
Backshell	387	0.148	366	0.140	-21	-5.36%
Descent Propellant	276	0.106	165	0.063	-111	-40.40%
Payload	725	0.277	860	0.329	135	18.66%
Other Systems	712	0.272	750	0.286	38	5.34%

class vehicle well with the only major difference between the two vehicles lying in the descent propellant. This discrepancy is to be expected based on the different terminal descent schemes used (*i.e.*, MSL using a sky-crane maneuver with a hover and divert phase, while the present investigation utilizes a constant thrust gravity turn.). The other major discrepancy lies in the heatshield mass, since MSL's heatshield is sized based on a 3σ dispersed trajectory, not a mass-optimal trajectory.

III.E.2. Human Class Mission

A previously published study,[2] was used to compare the applicability of the present sizing models to future, human class Mars missions. The study used for comparison investigated high mass human missions to Mars using 10 and 15 m Apollo-like entry capsules entering the atmosphere from a parking orbit following

aerocapture. The comparison case assumes a 10 m diameter vehicle with an L/D of 0.3 arrives at Mars with a mass of 40 t. After propulsive maneuvers following aerocapture and prior to entry, the system has a mass of 36.6 t at the entry interface. The vehicle descends through the Martian atmosphere and performs a propulsive gravity turn that targets an altitude of 50 m at 0 m/s. Following arrival at 50 m altitude, a 265 m/s divert maneuver is conducted in order to achieve a pre-defined landing target. Table 5 shows a comparison of the parameters used in the original and recreated investigation using the present models. Table 6 summarizes the comparative results.

Table 5. Human class and replicated vehicle parameters.

	Study by Christian, *et al.*	**This Investigation**
Entry Vehicle Shape	Apollo Capsule	70° Sphere-Cone
Entry Vehicle Diameter	10 m	10 m
Hypersonic L/D	0.3	0.3
Entry Mass	36,600 kg	36,600 kg
Inertial Entry Velocity	4.0 km/s	4.0 km/s
Inertial Entry Flight Path Angle	-14.5°	-14.5°
Nominal Design Atmosphere	30% 0 km MOLA MarsGRAM Atmosphere	Mars Pathfinder Reconstruction
Heating Regime	Laminar	Turbulent
Heatshield TPS Material	Carbon-Carbon	Heat Load Based Regression
Structure Mass	Forebody + Backshell: $0.25m_0$	Forebody: Dynamic Pressure Based Regression Backshell: $0.14m_0$
Supersonic Deceleration	Gravity Turn to $h = 50$ m, $V = 0$ m/s (Optimized Initiation)	Gravity Turn to $h = 50$ m, $V = 0$ m/s (Initiation at $M = 2.3$)
Divert Maneuver	265 m/s	265 m/s

Table 6. Comparison between human class and replicated vehicle sizing results.

	Study by Christian, *et al.*		**This Investigation**			
Component	*Mass [kg]*	$m_{component}/m_{entry}$	*Mass [kg]*	$m_{component}/m_{entry}$	*Mass Difference [kg]*	*% Difference*
Heatshield	4800	0.121	6341	0.159	1541	31.02%
Backshell	5000	0.125	5124	0.128	124	2.48%
Propulsion System	1400	0.035	1079	0.027	321	-22.91%
Descent Propellant	6400	0.160	6749	0.169	349	5.45%
Payload	10200	0.255	10145	0.254	-55	-0.54%
Other Systems	8760	0.219	7161	0.179	-1599	-18.25%

It can be seen that the two studies have similar results. Many of the currently sized components are within 10% of the original study's value with larger variations being seen for the heatshield, propulsion system, and other systems. The difference in heatshield mass is a direct result of the different aerothermal modeling assumptions. The study by Christian, *et al.*,[2] used a laminar stagnation point heating relation, whereas the current investigation implements a turbulent relationship. The propulsion system mass sizing difference is a result of the different optimization procedures used to determine the initiation point for terminal descent. The study by Christian, *et al.*,[2] optimized the initiation time of the gravity turn to provide minimize the total propulsion system mass; whereas, the present investigation examines initiation Mach numbers between Mach 2.5 and 3.0 to maximize payload mass. Due to the trade between thrust level (engine mass) and burn time (descent propellant), the present investigation results in a lower propulsion system mass but higher propellant mass than the study by Christian, *et al.*. Finally, the study by Christian, *et al.*,[2] carries 5% more dry mass margin than the current investigation, which is book kept in the other systems category, accounting for the discrepancy shown.

IV. Results and Discussion

IV.A. Delivered Payload Mass to Surface

The maximum payload mass fraction and mass (regardless of deceleration technology) obtained in this investigation are shown in Figure 8 for each entry mass, aeroshell shape, and entry velocity. Additionally, Figure 9 shows a representative set of subsystem mass breakdowns for the cases considered in this investigation. In

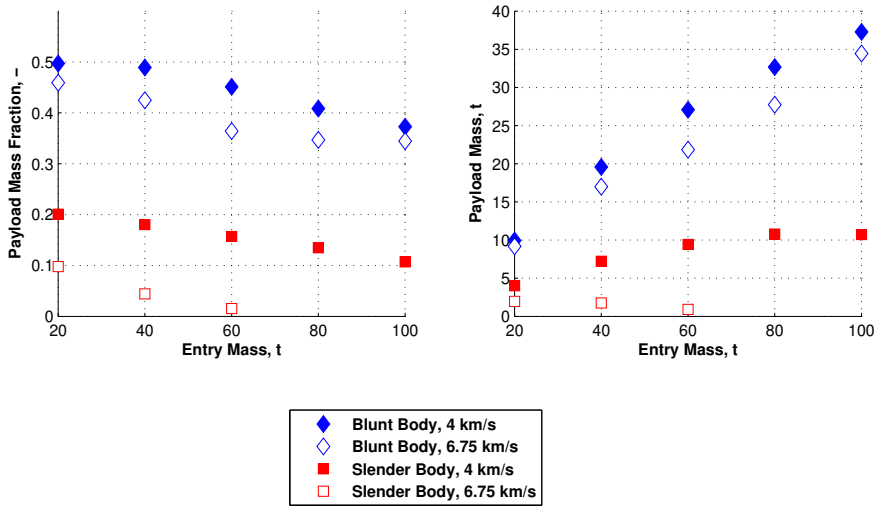

Figure 8. Maximum payload mass fraction and mass for different configurations and entry conditions.

Figure 8 it is observed that for the blunt body system, while the achievable payload mass fraction decreases as entry mass increases, the achievable payload mass monotonically increases. However, note that the incremental payload mass increase becomes less significant as the entry mass increases largely due to flight through a denser portion of the atmosphere increasing the heating and aerodynamic loading on the vehicle. The major implication of this observation, is that there exists a point where the payload mass is maximized. Extrapolating the trend demonstrated by the data, the maximum payload mass capable of being delivered by a blunt body system is approximately 41 t (occurring at a system entry mass of 141 t). The maximum payload mass demonstrated in this investigation occurs for a 100 t blunt body system at 37.3 t.

This performance is in contrast to the slender body 10 × 30 m ellipsled, which, based on data trends, may only be capable of delivering approximately 11 t of payload to the Martian surface (for an entry mass of 94 t), with 10.8 t being the maximum observed (for an entry mass of 80 t). While the ellipsled has more control authority and is capable of flying trajectories where the aerothermal and aerodynamic loading environment are relatively benign, the shear size (and resulting TPS and structural acreage) of the ellipsled provides an inherent disadvantage in sizing. This disadvantage is due to a multiplicative factor relative to the blunt body of approximately two for both the forebody structural and aftbody sizing relationships to account for the increased loading of the vehicle. Because the length of the structural members of the vehicle are substantially increased, the stress within these members for a given load are correspondingly larger. While being able to obtain (on average) a trajectory that has an integrated heat load $\sim$ 7 % less and a peak dynamic loading $\sim$ 5% less than that of the blunt body, the ellipsled does not provide the gains neeeded to compensate for its physical size disadvantage. As a result, the payload mass fraction achievable by the ellipsled is consistently $\sim$ 0.3 less than that of the sphere-cone.

Although the mass efficiency of the blunt body is better than that of the slender body for all cases considered, the packaging constraints of a high mass, blunt bodied system may preclude it from being implemented. For the maximum payload mass (37.3 t) observed in this investigation, an entry system packaging density of 404.5 kg/m^3 would be required, which is $\sim$ 16 % greater than that used by Apollo (the maximum historical payload density achieved). In addition, a slender body system, such as the ellipsled, may have other architectural advantages, such as the ability to accommodate large volume payloads and the

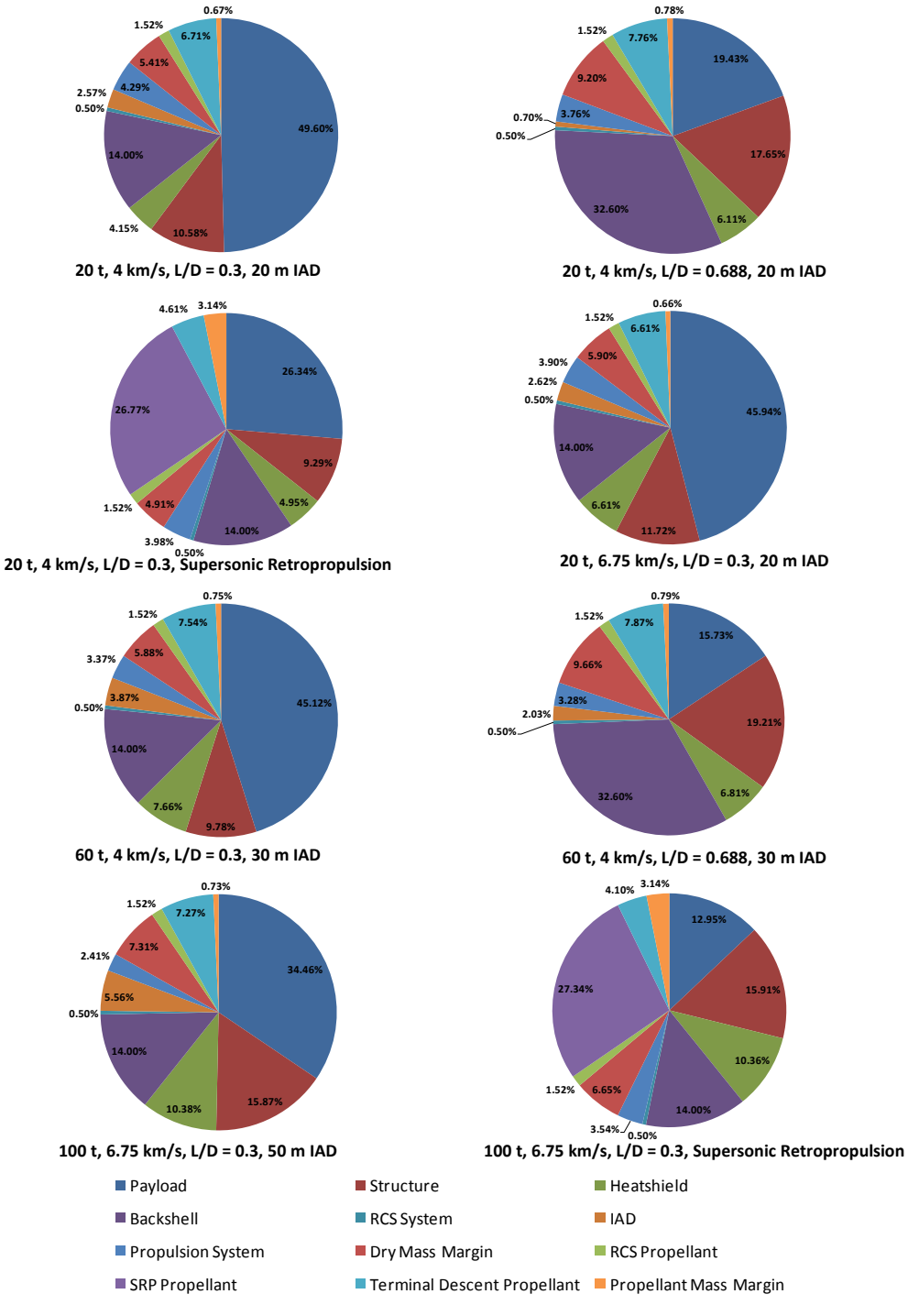

Figure 9. Subsystem mass percentages for various representative entry configurations.

potential for use in a multi-functional manner (*e.g.*, additional use as a launch shroud or a surface habitat).

Also noticeable in Figures 8 and 9 is the difference between entry from orbital (4 km/s) and direct (6.75 km/s) velocities. For the blunt body, there is a payload mass fraction penalty of ~ 0.05 for entering directly from orbit, while the payload mass fraction penalty for the slender body is more pronounced at ~ 0.10. This penalty is due to two effects, increased heat load ($\sim 35\%$) required to dissipate the increased energy of the vehicle and higher loads (2-5 times that of entry from orbit) placed on the forebody of the vehicle. As a

result of the increased acreage of the slender body, this mass penalty does not allow the slender body to decelerate entry masses greater than 60 t from direct entry conditions.

IV.B. Impact of the Supersonic Deceleration Technology

Figures 10-13 are a more detailed view of Figure 8, in which supersonic decelerator performance is examined to identify appropriate regimes of applicability. Each figure contains results assuming one of four supersonic decelerators—20 m diameter tension cone IAD, 30 m diameter tension cone IAD, 50 m diameter tension cone IAD, and supersonic retropropulsion.

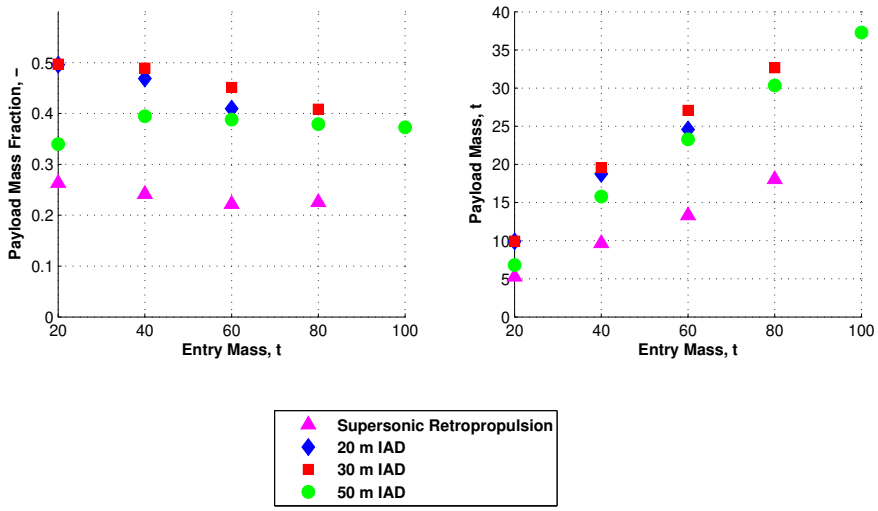

Figure 10. Landed mass performance for the blunt body entering from orbit using various supersonic deceleration technologies.

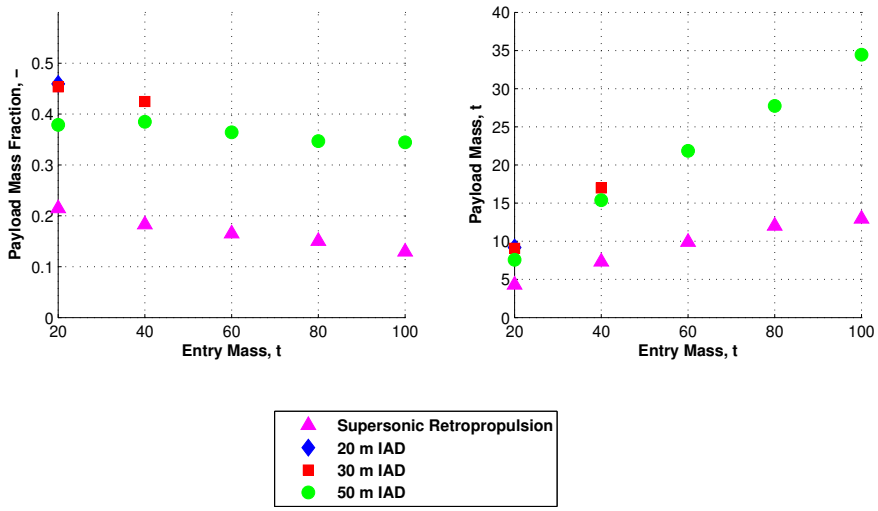

Figure 11. Landed mass performance for the blunt body with direct entry using various supersonic deceleration technologies.

For the blunt body system, Figures 10 and 11, illustrate regimes of appropriate IAD diameter usage as a function of entry mass. In particular, for the entry from orbit cases with entry masses less than 60 t there

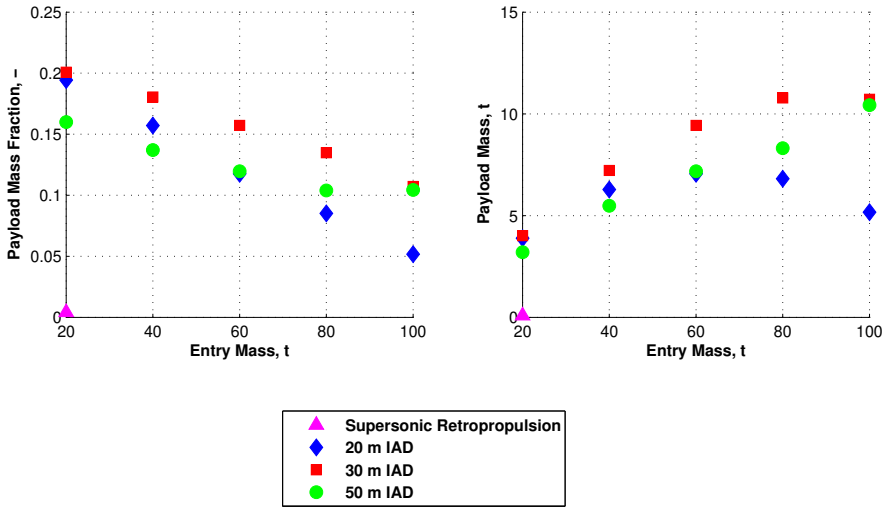

Figure 12. Landed mass performance for the slender body entering from orbit using various supersonic deceleration technologies.

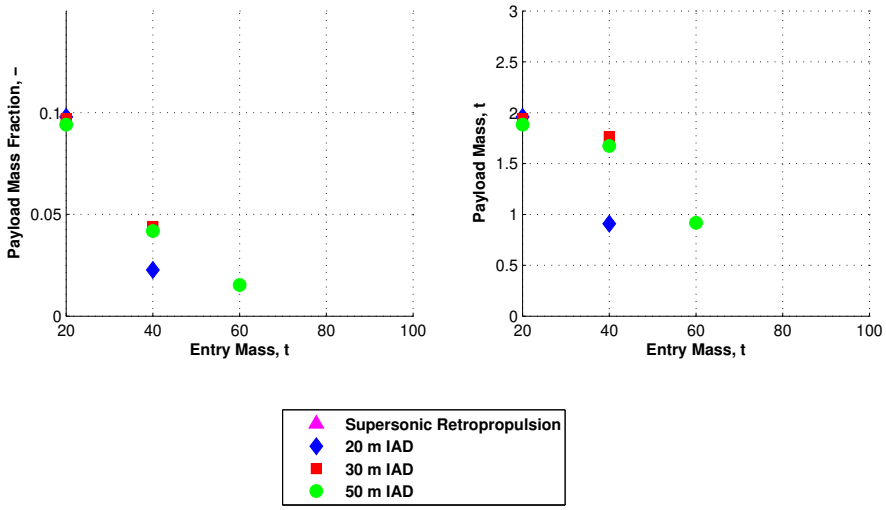

Figure 13. Landed mass performance for the slender body with direct entry using various supersonic deceleration technologies.

is approximately equal performance seen by the 20 m and 30 m diameter IADs (implying that the 20 m diameter IAD would suffice). While for entry masses greater than 60 t, a 20 m diameter IAD is no longer capable of decelerating the system due largely to the increased ballistic coefficient not allowing adequate timeline to stage to the subsonic propulsive terminal descent phase. For entry masses greater than 80 t, only a 50 m diameter IAD is capable of delivering payload to the Martian surface. For the direct entry cases, the 20 m IAD is only sufficient for entry masses below 20 t; whereas, for entry masses greater than 40 t, a 50 m IAD is required to deliver sufficient drag deceleration.

Using supersonic retropropulsion for the blunt body has a payload mass fraction penalty of ~ 0.25 for all entry conditions (mass and velocity) considered in which payload can be delivered to the Mars surface. This mass penalty is attributed to the propellant required by the system during the deceleration requiring significantly more mass than the IAD ($\sim$ 8 times the mass of the corresponding IAD). While supersonic

retropropulsion provides a lighter vehicle at the time of staging to terminal descent, this mass difference is not significant enough for the short burn time of the subsonic gravity turn to have a substantial impact. In fact, for the slender body cases, seen in Figures 12 and 13, this increased propellant mass precludes any payload from reaching the surface.

In this investigation, a maximum thrust-to-weight ratio of 3.0 was assumed. For the blunt body entering from orbit, this thrust-to-weight limit prohibits delivering payload to the surface for entry masses greater than 80 t. However, should the thrust-to-weight ratio be increased to 6.0, a solution does exist for an entry mass of 100 t, which delivers 19 t of payload.

As seen in Figure 11, supersonic retropropulsion benefits from the increased dynamic pressure seen during the supersonic phase of flight for direct entry cases as it is capable of delivering payload to the surface for all entry masses. There exists some drag benefit for operating in increased dynamic pressure regimes as this lowers the thrust coefficient (other conditions being equal) and there is more deceleration for a given amount of thrust. Examination of the thrust profiles show a tendency for the system to use a small-to-moderate amount of thrust initially (benefiting from some preservation of drag) and ramping up the thrust level towards the end of the trajectory where the thrust coefficient is required to be too high to achieve benefits from drag preservation.[26] The importance of drag preservation becomes less pronounced as entry mass is increased because the thrust dominates the aerodynamic forces acting upon the vehicle, corroborating the supersonic retropropulsion performance results described by Korzun and Braun.[22]

Figure 14 shows the optimized trajectories of a blunt body with an entry mass of 20 t entering from orbit for each of the supersonic decelerator options considered. Superimposed on this figure are altitude-velocity bounds which show the region where supersonic retropropulsion has some degree of aerodynamic drag preservation (based on subsonic altitude, Mach number, and dynamic pressure constraints).[22]

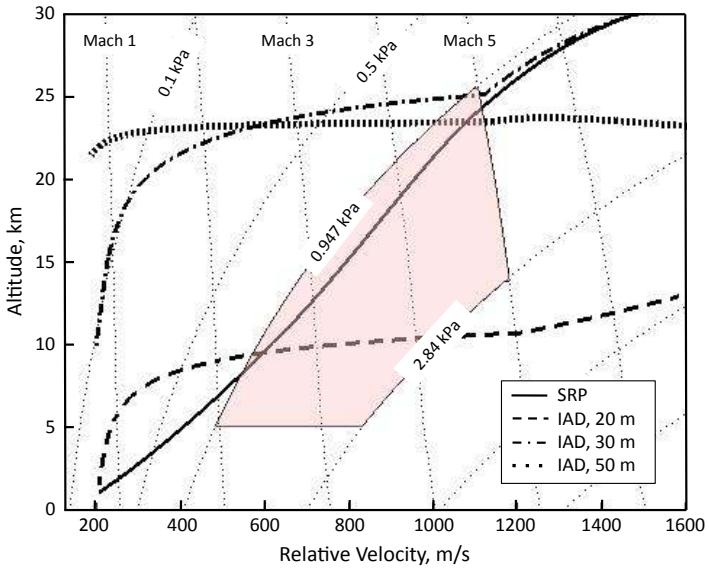

Figure 14. Trajectories for the various decelerators for the 20 t entry mass, blunt body, entry from orbit case.

Note that the supersonic retropropulsion solution obtained does not correspond to the minimum propellant mass solution as a result of the overall system sizing. To minimize propellant usage, it would be desirable to initiate the supersonic retropropulsion phase at as low of an altitude and velocity as possible; however, initiating the supersonic retropropulsion phase in this manner increases both the heat load (TPS mass) and peak dynamic pressure (structural mass). At the system level, decreasing the structural and TPS subsystem mass outweighs the potential propellant savings. The IAD trajectories, as can be expected, terminate at increasing altitudes for increasing diameters. The 30 m and 50 m IAD deploy at approximately the same condition with the 20 m IAD deploying closer to the surface than the other two. This effect again represents the trade between the system level objectives and the decelerator objectives as the savings in terminal descent propellant required by the 20 m diameter case outweighs the additional mass of the other system masses found by deploying at a higher dynamic pressure. The larger diameter IADs would have a more severe mass

penalty for deployment in the higher dynamic pressure enviroment.

IV.C. Impact of Ellipsled Size

As discussed previously, the 10 × 30 m ellipsled (used in the Mars Design Reference Architecture 5.0[3]) has a mass penalty associated with its use due to the vast size of the vehicle. Relative to the blunt body, this large size leads to low packaging densities relative to the sphere-cone. In fact, even for the 100 t entry mass, the packaging density is approximately an order of magnitude less than that achieved by Apollo. To examine the effect of larger packaging density on the slender body configuration, the ellipsled was photographically scaled such that its aerodynamic performance was maintained. The performance of two smaller vehicles is considered, a 8 × 24 m ellipsled and a 6 × 18 m ellipsled, for a 20 t entry mass with a 20 m diameter IAD entering from orbit. This results in a packaging density of 17.6 kg/m^3 and 41.6 kg/m^3 for the 8 × 24 m and 6 × 18 m ellipsleds, respectively. As vehicle diameter is reduced, the drag area is also reduced causing an increase in the ballistic coefficient. For a diameter reduction from 10 m diameter to 6 m, the ballistic coefficient increases by a factor of approximately three (from 149 kg/m^3 to 413 kg/m^3), a change which will significantly alter the flight mechanics of the vehicle. Additionally, because heat rate is approximately proportional to the inverse square root of the effective nose radius and proportional to ballistic coefficient, the aerothermal heating (both peak heat rate and integrated heat load) will increase as vehicle size is reduced.

Figure 15 shows the impact of these effects on the multiplicative factor on the structural and backshell sizing models, Eqs. (3) and (5) ($k_{\text{structure}}$ and $k_{\text{backshell}}$), and the fraction of the entry mass for structure, backshell, TPS, and payload. The most profound effect observed as vehicle size is reduced is the doubling

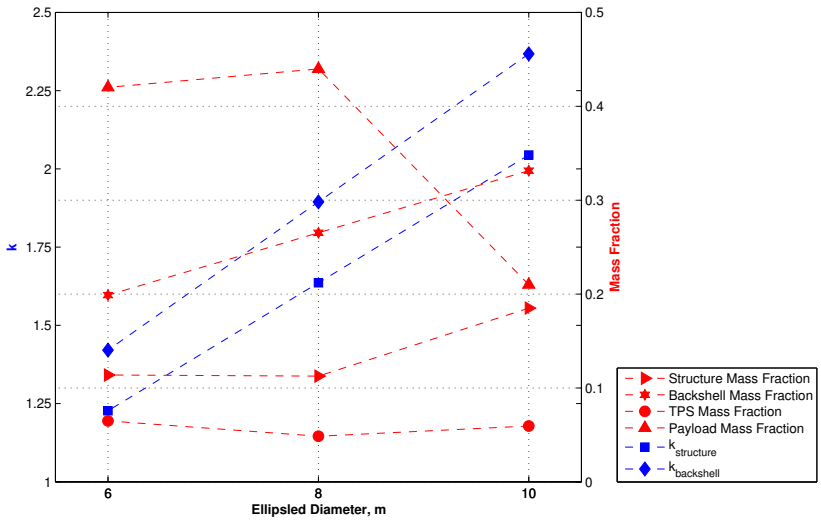

Figure 15. Effect of photographically scaling the baseline 10 × 30 m ellipsled.

of landed payload performance—from 4.2 t to 8.4 t (from 21% to 42% payload mass fraction). Note that the maximum payload mass occurs for the 8 × 24 m ellipsled, implying that there is an optimal size for a given entry condition. This is likely a significant consideration for even higher entry masses such as those under consideration for human Mars exploration.[3] This optimal size results from the manner in which the trajectory affects the structural and TPS sizing. For example, the structural mass fraction remains approximately constant between the 8 × 24 m and 6 × 18 m ellipsled despite a reduction in the structural multiplicative factor from 1.63 to 1.23. This is due to increased aerodynamic loading on the vehicle as a result of the increased ballistic coefficient.

IV.D. High Mass Mars EDL Technology Requirements

Based upon the results of this investigation, the required EDL technology set as a function of landed mass can be listed based on the regimes in which these systems are best applied. This compilation is provided in

Table 7.

Table 7. Mars EDL technology requirements for various payload masses.

	∼ 20 t Payload	∼ 40 t Payload	∼ 80 t Payload
Entry Mass	≥ 40 t	> 100 t	> 200 t
Aeroshell Diameter	∼ 10 m	≥ 10 m	>> 10 m
Aeroshell Shape	Blunt Body or Scaled Slender Body	Blunt Body	Unknown
Structural and TPS Material	Historical	Historical or New Lightweight Development Program	New Lightweight Development Program
Entry Velocity	Orbital or Direct	Orbital	Orbital
Supersonic Deceleration	≥ 20 m IAD or Supersonic Retropropulsion	≥ 50 m IAD	> 50 m IAD

As can be seen from this summary table, as the required payload mass increases the severity of the deviation from traditional Mars EDL technology increases. For the 20 t payload, both 10 m diameter blunt and slender body solutions likely exist with supersonic deceleration options that include reasonable IAD diameters (≥ 20 m) or the use of supersonic retropropulsion. Additionally, both direct and orbital entry velocities are likely to provide acceptable solutions. For this case, the performance curve of the slender body from orbit shows promise of achieving 20 t payloads, particularly in light of the discussion on scaling the vehicle to increase the packaging density.

As the payload mass increases from 20 t to 40 t, the technology challenges increase drastically. For example, a very large diameter IAD (≥ 50 m) is required to provide sufficient supersonic deceleration. In addition, for a 40 t payload mass, a 10 m diameter blunt body is shown to be marginally sufficient when entering from orbit. However, the packaging density required for such a system to decelerate this payload is beyond that ever flown. Neither the direct entry or slender body cases appear feasible.

For an 80 t payload, no solutions were obtained. Such an EDL system is likely well beyond our current capabilities and an entry mass > 200 t is likely required. This EDL system will likely require an entry vehicle diameter significantly larger than 10 m and an IAD diameter above 50 m. Packaging density constraints will likely prohibit a blunt body from consideration for this payload class. Furthermore, the vehicle's structure and TPS will need to be composed of advanced lightweight materials, unlike those currently used.

IV.E. Model Sensitivity

An investigation into the sensitivity of these results to modeling assumptions and uncertainties was undertaken. For this investigation the 40 t, 30 m IAD, entry from orbit case was analyzed by perturbing each of the sizing models by +10% and reoptimizing the design variables to maximize the payload mass. The result is then compared with the nominal case and plotted in Figure 16.

Due to the slender body carrying significantly less payload (54%), the ellipsled has much higher sensitivity to each of the subsystem models. In particular, the subsystems that nearly trade on a one-to-one basis with payload (backshell, structure, and propulsion) must be better understood for the ellipsled than for the sphere-cone. For instance, consider the 100 t slender body vehicle entering from orbit with a 30 m IAD. By reducing the structure and backshell multiplicative factors, $k_{\text{structure}}$ and $k_{\text{backshell}}$, to unity, the payload mass increases from 10.7 t to 40.4 t. Note that this mass is consistent with the payload mass achieved by the Mars Design Reference Architecture 5.0[3] for similar entry masses. In contrast, the subsystems whose sizing affects the initial mass remaining for the propulsive descent (*e.g.*, IAD and TPS) are of less significance.

An additional investigation into the sensitivity of the entry system delivery accuracy was performed by analyzing the impact of a ±0.14° variation in entry flight path angle, commiserate with that required by the MER system.[27] This analysis used the 20 t direct entry vehicle with a 20 m diameter IAD. The flight path angle obtained during the original optimization was perturbed by the desired ±0.14° and the design was reconverged with flight path angle removed as a design variable. Since the bank angles remain free design variables, this approach simulates an on-board guidance system. For this flight path angle variation, the payload mass varied by just 18 kg (0.2% of the original payload). As such, the mass breakdown is estimated to be relatively insensitive to flight path angle variations.

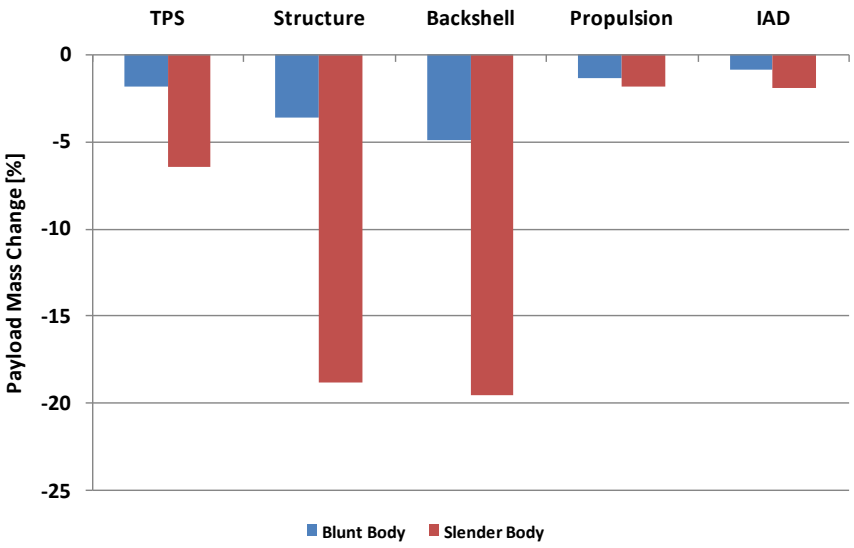

Figure 16. Sensitivity of a 40 t, 30 m IAD vehicle entering from orbit to a +10% change in sizing models.

V. Conclusions

This investigation identified and evaluated several key system trades associated with landing high mass payloads at Mars. Principally, these are the trades associated with supersonic deceleration and the entry vehicle's shape. Through these trades, it was seen that a maximum payload of the order of 37 t is capable of being delivered from entry vehicles ranging in mass between 20 and 100 t. Assuming a 10 m aeroshell diameter, the maximum landed mass possible for the blunt body configuration is estimated to be 41 t; however, this required an entry mass on the order of 140 t which would significantly exceed the largest packaging density achieved to date (Apollo). A payload mass fraction penalty of $\sim$ 0.05-0.10 was shown to exist for entering directly from the interplanetary transfer as opposed to from orbit, due to the increased aerothermal and aerodynamic loads imparted onto the vehicle. In addition, the blunt 70° sphere-cone aeroshell demonstrated a payload mass fraction improvement of $\sim$ 0.3 relative to the slender ellipsled. This is due to the sphere-cone's size advantage (structural and TPS acreage) which was not compensated for by the increased control authority of the ellipsled. However, this investigation also demonstrated that the ellipsled configuration may be improved by optimizing its size, as a result of the manner in which the trajectory impacts the structural and TPS sizing. Finally, it was shown that supersonic retropropulsion delivered less payload than the tension cone IAD in all cases, with supersonic retropropulsion benefiting little from the impact of drag preservation under current modeling and configuration assumptions.

Acknowledgments

The authors would like to thank the National Aeronautics and Space Administration (NASA) who funded the work discussed here as part of the Reentry Aerothermodynamics Virtual Institute of the Constellation University Institutes Project (CUIP). The insight provided by Walt Engelund and others at NASA Langley Research Center and Mike Wright at NASA Ames Research Center has been invaluable. Collaboration with John Christian allowed the comparison to the previous human Mars exploration system study to be possible and is greatly appreciated. Finally, the authors would like to thank their colleagues within the Space Systems Design Laboratory at Georgia Tech who have also contributed to this work—Zarrin Chua, Allison Hutchings, and Christopher Marsh.

References

[1]Braun, R. D. and Manning, R. M., "Mars Exploration Entry, Descent, and Landing Challenges," *Journal of Spacecraft and Rockets*, Vol. 44, No. 2, 2007, pp. 310–323.

[2]Christian, J., Wells, G., Lafleur, J., Verges, A., and Braun, R., "Extension of Traditional Entry, Descent, and Landing Technologies for Human Mars Exploration," *Journal of Spacecraft and Rockets*, Vol. 45, No. 1, 2008, pp. 130–141.

[3]Drake, B. G., "Human Exploration of Mars: Design Reference Architecture 5.0," *NASA SP-2009-566*, July 2009.

[4]Cruz, J. R. and Lingard, J. S., "Aerodynamic Decelerators for Planetary Exploration: Past, Present, and Future," *AIAA 2006-6792, 2006 AIAA Guidance, Navigation and Control Conference and Exhibit*, Keystone, CO, Aug. 2006.

[5]Clark, I., Hutchings, A., Tanner, C., and Braun, R., "Supersonic Inflatable Aerodynamic Decelerators For Use on Future Robotic Missions to Mars," *Journal of Spacecraft and Rockets*, Vol. 46, No. 2, 2009, pp. 340–352.

[6]Korzun, A., Cruz, J., and Braun, R., "A Survey of Supersonic Retropropulsion Technology for Mars Entry, Descent, and Landing," *IEEEAC 1246, 2008 IEEE Aerospace Conference*, Big Sky, MT, March 2008.

[7]Steinfeldt, B. A., Grant, M. J., Matz, D. A., Braun, R. D., and Barton, G. H., "Guidance, Navigation, and Control Technology System Trades for Mars Pinpoint Landing," *AIAA 2008-6216, 2008 AIAA Atmospheric Flight Mechanics Conference*, Honolulu, HI, Aug. 2008.

[8]Heneman, W., "Fundamental Techniques of Weight Estimation and Forecasting for Advanced Manned Spacecraft and Space Stations," *NASA TN D-6349*, May 1971.

[9]Kinney, D. J., "Aero-Thermodynamics for Conceptual Design," *AIAA 2004-13382, 2004 AIAA Aerospace Sciences Meeting and Exhibit*, Reno, NV, Jan. 2004.

[10]Spencer, D. A., Blanchard, R. C., Braun, R. D., Kallemeyn, P. H., and Thurman, S. W., "Mars Pathfinder Entry, Descent, and Landing Reconstruction," *Journal of Spacecraft and Rockets*, Vol. 36, No. 3, 1999, pp. 357–366.

[11]Stiepe, S. A., Powell, R. W., Desai, P. N., Queen, E. M., Brauer, G. L., Cornick, D. E., Olson, D. W., Petersen, F. M., Stevenson, R., Engel, M. C., Marsh, S. M., and Gromko, A. M., "Program to Optimize Simulated Trajectories (POST II) Utilization Manual," *Version 1.1.6.G*, Hampton, VA, Jan. 2004.

[12]Sutton, K. and Randolph A. Graves, J., "A General Stagnation-Point Convective-Heating Equation for Arbitrary Gas Mixtures," *NASA TR R-376*, Nov. 1971.

[13]Edquist, K. T., Dyakonov, A. A., Wright, M. J., and Tang, C. Y., "Aerothermodynamic Environments Definition for the Mars Science Laboratory Entry Capsule," *AIAA 2007-1206, 2007 AIAA Aerospace Sciences Meeting and Exhibit*, Reno, NV, Jan. 2007.

[14]Tauber, M. E., "A Review of High-Speed Convective, Heat-Transfer Computational Methods," *NASA TP 2914*, 1989.

[15]Davies, C., "Planetary Mission Entry Vehicle Quick Reference Gude, Version 3.0," *NASA SP-2006-3041*, 2006.

[16]Laub, B. and Venkatapathy, E., "Thermal Protection System Technology and Facility Needs for Demanding Future Planetary Missions," *International Workshop on Planetary Probe Atmospheric Entry and Descent Trajectory Analysis and Science Proceedings*, Lisbon, Portugal, Oct. 2003.

[17]Hoffman, S. J. and Kaplan, D. L., "Human Exploration of Mars: The Reference Mission Mission of the NASA Mars Exploration Study Team," *NASA SP-6107*, July 1997.

[18]Drake, B. G., "Reference Mission 3.0, Addendum to the Human Exploration of Mars: The Reference Mission Mission of the NASA Mars Exploration Study Team," *NASA EX13-98-036*, June 1998.

[19]Clark, I. G., *Aerodynamic Design, Analysis and Validation of a Supersonic Inflatable Decelerator*, Ph.D. thesis, Georgia Institute of Technology, Atlanta, GA, Aug. 2009.

[20]Jarvinen, P. and Adams, R., "The Aerodynamic Characteristics of Large Angled Cones with Retrorockets," *NASA Contract NAS 7-576*, Feb. 1970.

[21]Keyes, J. and Hefner, J., "Effect of Forward Facing Jets on Aerodynamic Characteristics of Blunt Configurations at Mach 6," *Journal of Spacecraft and Rockets*, Vol. 4, No. 4, 1967, pp. 533–534.

[22]Korzun, A. M. and Braun, R. D., "Performance Characterization of Supersonic Retropropulsion for Application ot High-Mass Mars Entry, Descent, and Landing," *AIAA 2009-5613, 2009 AIAA Atmospheric Flight Mechanics Conference*, Chicago, IL, Aug. 2009.

[23]Larson, W. J. and Pranke, L. K., *Human Spaceflight: Mission Analysis and Design*, Mc-Graw Hill, 1999.

[24]"Constellation Program Human-Systems Integration Requirements (HSIR)," *NASA CxP-70024*, Jan. 2007.

[25]Wolf, A., Tooley, J., Ploen, S., Gromov, K., Ivanov, M., and Acikmese, B., "Performancce Trades for Mars Pinpoint Landing," *IEEEAC 1661, 2006 IEEE Aerospace Conference*, Big Sky, MT, March 2006.

[26]Marsh, C. L. and Braun, R., "Fully-Propulsive Mars Atmospheric Transit Strategies for High-Mass Payload Missions," *IEEEAC 1219, 2009 IEEE Aerospace Conference*, Big Sky, MT, March 2009.

[27]Potts, C. L., Raofi, B., and Kangas, J., "Mars Exploration Rovers Propulsive Maneuver Design," *AIAA 2004-4985, 2004 AIAA/AAS Astrodynamics Specialist Conference and Exhibit*, Providence, RI, Aug. 2004.